Targeted Rework Strategies for Powder Bed Additive Manufacture

M. Hirsch[a,b], P. Dryburgh[a,b], S. Catchpole-Smith[b], R. Patel[a], L. Parry[c] , S.D. Sharples[a], I.A. Ashcroft[c] and A.T. Clare[b,*]

[a]Optics and Photonics Group, Faculty of Engineering, The University of Nottingham, Nottingham, NG7 2RD, U.K.
[b]Advanced Component Engineering Laboratory, Faculty of Engineering, The University of Nottingham, Nottingham, NG7 2RD, U.K.
[c]Centre for Additive Manufacturing, Faculty of Engineering, University of Nottingham, Nottingham, NG7 2RD, U.K.

Abstract

A major factor limiting the adoption of powder-bed-fusion additive manufacturing for production of parts is the control of build process defects and the effect these have upon the certification of parts for structural applications. In response to this, new methods for detecting defects and to monitor process performance are being developed. However, effective utilisation of such methods to rework parts in process has yet to be demonstrated.

This study investigates the use of spatially resolved acoustic spectroscopy (SRAS) scan data to inform repair strategies within a commercial selective laser melting machine. New methodologies which allow for rework of the most common defects observed in selective laser melting (SLM) manufacturing are proposed and demonstrated. Three rework methodologies are applied to targeted surface breaking pores: a hatch pattern, a spiral pattern and a single shot exposure. The work presented shows that it is possible to correct surface breaking pores using targeted re-melting, reducing the depth of defects whilst minimising changes in local texture. For the hatch rework and spiral rework, a reduction in defect depth of 50 % and 31 % were observed, respectively, however, no improvement was seen after the single shot exposures. This work is part of a programme to develop a method by which defects can be detected and the part reworked in-process during SLM to enable defect specification targets to be met. Although further work in developing build-characterise-rework strategies for integrated and targeted defect correction is needed, the feasibility of the underlying method of identifying and selectively reworking to reduce a defect has now been demonstrated for the first time.

Keywords: non-destructive evaluation, additive manufacture, selective rework, selective laser melting

1. Introduction

Selective laser melting (SLM) is a powder-bed-fusion additive manufacturing (AM) process that is being increasingly considered as an alternative to current manufacturing methods in a number of high value-added industries [1-4]. However, this technology is still hindered by an inability to guarantee component build quality alongside a lack of robust inspection techniques suited to AM components [5]. Part integrity is associated with the presence of surface and subsurface micro defects, which cannot currently be reliably predicted or controlled for SLM. The reduction of these defects to a level consistent with a specified structural integrity is necessary if SLM is to be adopted for components operating in safety critical applications.

One of the most common defects to occur in powder-bed-fusion is porosity, which act as stress concentration sites and have been shown to significantly reduce the fatigue [6] and elongation [7] performance in SLM components [8]. Furthermore porosity negates the mechanical benefit offered by

the finer lamellar microstructure characteristic of SLM by reducing the yield strength [7]. It has been shown that these voids can present in a range of sizes, <5 – 500 μm [9], and can either spread throughout the bulk or be located primarily between the internal hatching area and the external border [10]. Further investigations have developed a classification system for porosity based on morphology which relates defects to processing parameters; spherical pores caused by gas entrapment, or acicular pores due to lack of fusion between layers. As such, component defects occur as a function of processing parameters, material feedstock and build methodology, for example a lack of material fusion due to incorrect laser power, impurities in the feedstock or improper gas flow [11-14]. The definition of a critical defect size, resulting in scrappage of the component, is industry and application dependent [15]. Better understanding of the root causes of such defects in SLM components is a focus of ongoing research. However, the large number of process parameters (>50) [16] and inter-dependency between complex effects such as denudation, and material spattering [17] mean, despite many studies in process optimisation, it is still impossible to predict or control defect size and distribution. As stated by Leuders et al. the development of porosity defects during fabrication cannot be avoided currently [8].

As these defects cannot be avoided several techniques have been developed by the industry to optimise AM part integrity. For example, Hot Isostatic Pressing (HIPing) is currently a common post-processing technique for reworking internal porosity in superalloy components. However, it has been shown that this costly additional step is not capable of closing surface connected pores [18]. Furthermore, accurate control of the surface microstructure is not possible [19]. Previously, laser re-melting by applying additional skin scans has been employed to improve surface roughness [20, 21]. It was shown, however, that compressive residual stresses were created as a consequence of this re-melting process. Further to this, Yasa et al. [22] showed that complete layer re-melting for defect rework on steel SLM components could reduce near surface porosity, but at the expense of a change in microstructure akin to a recast layer. This approach has been reported to yield SLM parts with unpredictable and anisotropic microstructures [23]. Mireles et al. [24] used infra-red imaging for in-situ monitoring in a selective electron beam melting process, reworking artificial defects in Ti-6Al-4V components via large area re-melting. It was shown that re-melting successfully restored component integrity, however the authors used two inspection methods, thermography and X-ray computed tomography for defect sizing, yielding significantly different results, thus the efficacy of re-melting the artificial defects remains unclear. Furthermore, the defects seeded in the component were an order of magnitude greater than those seen to commonly occur in SLM in practice.

This necessitates research into both identifying and correcting such defects. As reported by Everton et al. [9], in-situ non-destructive evaluation (NDE) techniques have been subject to rapid development for use in AM processes. It was concluded that there was a clear industrial pull for in-situ monitoring, particularly for technologies that could be coupled with a form of closed-loop feedback to optimise processing parameters. In a closed loop system, an automated decision can be made to i) scrap the build – saving valuable build time and material – or preferably ii) enact an on-the-fly rework to allow completion of the part [15]. It has been proposed that spatially resolved acoustic spectroscopy (SRAS) is an NDE technique that is well suited to inspect SLM components, based on the capability to inform upon microstructural texture of the part [25], the ability to differentiate between surface and sub-surface defects [26], and potentially measure rough surfaces [27]. SRAS is a laser ultrasound technique which uses surface acoustic waves (SAWs) to probe the elastic properties of the sample in order to determine crystallographic orientation information, whilst additionally generating a separate optical image; the technique and instrumentation is described in previous work [28, 29].

The focus of this study is to show defects, identified using NDE techniques at the surface of a given layer, can be reworked using defined scan strategies. SRAS is utilised in this study to locate and characterise surface defects and a number of targeted rework strategies are investigated for their ability to repair the defect. The reduction in the size of an array of defects within an SLM build subjected to these various strategies is then presented. Information on the defect type, location and morphology

measured pre- and post-rework is shown, along with a texture map. Finally, a methodology in which the proposed technique can be integrated into SLM builds to guarantee part integrity is discussed.

2. Methodology

SLM test samples were manufactured using a ReaLizer SLM50 with the nickel superalloy, Inconel 718, the composition of which can be found in the literature [30]. A 10×10×10 mm cube was built using a meander scan strategy with a hatch spacing of 60 µm and a 67° rotation between each layer. A laser power of 100 W, spot size of 40 µm and scanning speed of 560 mms^{-1} were used to build layer thicknesses of 40 µm. Gas atomised powder sized 15−45 µm (measured with a Malvern Mastersizer 3000) was used as the powder feedstock.

After manufacture, the sample was polished to an average R_a ~100 nm prior to inspection by SRAS and optical microscopy. The SRAS system operates on a raster-point scan principle [28]. Each point was obtained by pulsing (T=1-2 ns) a 1064 nm Q-switched laser (AOT-YAG-10Q) (generation laser) through an optical grating at a repetition frequency of 2 kHz. As a result, a surface acoustic wave (SAW) is generated. The SAW is detected with a split photodiode using a 532 nm continuous wave laser (Laser Quantum Torus 532). Measurement of the frequency of each SAW packet allows calculation of the velocity of the wave, which can be used to output an image showing texture contrast. The generation patch size was ~200 µm, giving an acoustic image resolution of ~100 µm. In addition to obtaining velocity information, the system recorded an optical dataset of the measured surface; the optical image resolution being 10 µm/px. The prepared surfaces were also imaged using a focus variation microscope (Alicona InfiniteFocus G5) with a 20× lens and in-built image stitching tool. The lateral and vertical resolution of the 3D micrographs was 2.94 µm/px and 0.1 µm/px, respectively. The original build parameters were reused for the rework operation. In order to solely investigate the effect of re-melting, no additional powder was used in the rework process.

Three pore rework strategies were investigated, as shown in the schematic presented in 1: A hatch melting pattern, a spiral melting pattern and single shot melting for pores similar in size to the laser spot size. A single shot exposure was defined for defects ranging in sizes of 20-40 µm, with the laser being centred on the defect. A minimum and maximum exposure time of 30 µs and 100 µs, respectively, was defined based on standard manufacturing parameters. An exposure time of 95 µs was calculated for an exemplary defect of ~40 µm whilst scaling this for larger defects. The hatch melting pattern was selected since the samples were manufactured identically. The spiral melting pattern was proposed by Jhabvala et al., showing optimised thermal gradients in both the x and y direction designed to avoid overheating [31]. Since re-melting hatch patterns are based on the size of defects (~<500 µm), assuming optimised working parameters, more complex melting patterns such as fractal scans, chessboard scanning and ‘paintbrush’ scanning are not feasible as these are designed for bulk part processes.

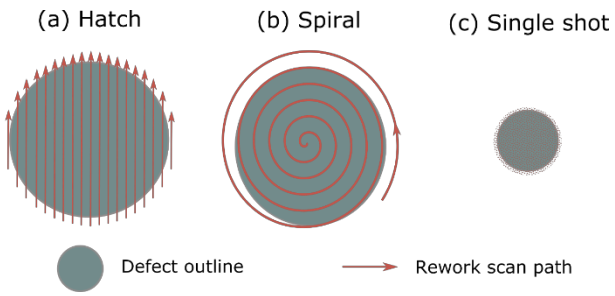

Figure 1: Scan strategies for pore rework trialled in this work: (a) a simple hatch pattern as used in the manufacture of a part; (b) a spiral scan pattern where the gap between the scan lines is equal to a single hatch spacing; (c) discrete single shot exposures for defects smaller than the laser spot diameter, 20-40 µm.

In order to generate rework paths, an automated algorithm was developed, based on the flow chart in 2. The original optical SRAS data is shown in 2(a). A size thresholding step was then used to disregard defects and outliers smaller than 20 µm from the SRAS optical scan data, shown in 2(b), given the image resolution of 10 µm (pixel size) and the defined minimum cluster size of 2×2 pixels [15]. This step can be adjusted to ensure that only those defects that take the part out of specification are reworked. A filtering step, based on eroding and dilating, closes non-uniform surface defects, 2(c). This step is necessary for avoiding partial or uncontrolled splitting of hatch patterns on a targeted defect. The resultant binary image from these steps is then processed to segment defects based on their aspect ratio; the centroid and dimensions are obtained, 2(d), to only target pores. The final processing step is the generation of the rework paths, 2(e). In this step the rework area is defined by dilating the defect area by 150%. The laser path vector spacing for both hatch and spiral rework was defined as 40 µm and is based on standard manufacturer parameters for Inconel 718 (~40-60 µm). All scan strategies were defined from the outer edge of the defect inwards, in order to draw material into the defect. The 150% rework area was selected in order to process sufficient re-melt material to reduce the defect size whilst not interfering with neighbouring defect rework areas. An example rework path as created by the algorithm is shown in 2(f), with a zoom of the highlighted sector in 2(e). The resulting vector rework paths were then verified through simulation in the ReaLizer RDesigner software to ensure data integrity.

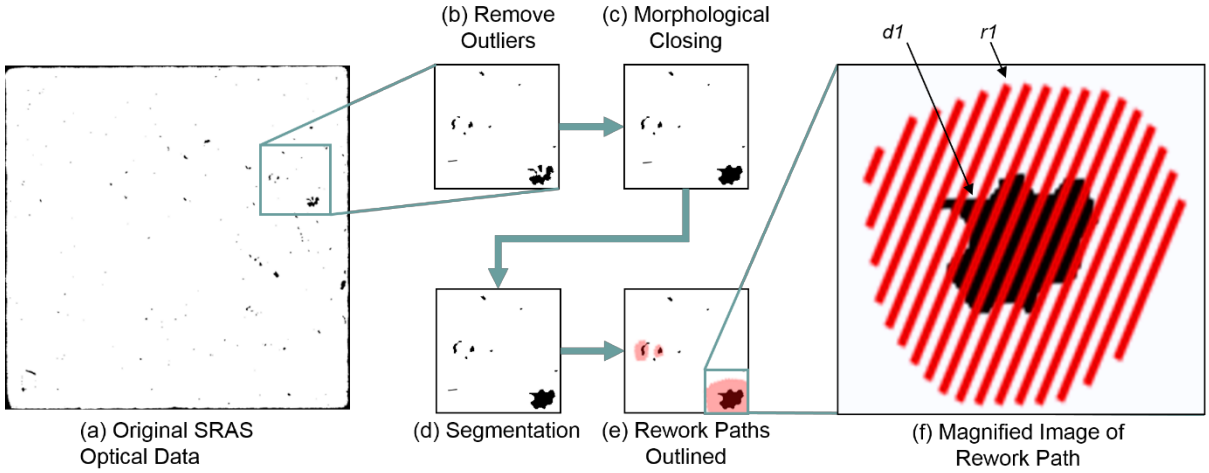

Figure 2: Micrograph analysis steps outlining the order of operations for preparation of pores for rework: (a) the original optical data set; (b) removing outliers (defects < 20 µm); (c) morphological closing based on eroding and dilating the binary image; (d) segmentation based on their aspect ratio and centroid for determination of dimensions and location; (e) the rework paths are created and overlaid; (f) magnified image of rework area showing individual hatch lines. The defect highlighted has been denoted *d1* and its respective rework path has been denoted *r1*.

3. Results and Discussion

To show the efficacy of the rework, focus variation micrographs of the samples were obtained before and after the rework was conducted, to extract defect depth profiles. In order to define a successful rework the height difference between the surface and defect depth should be significantly reduced. It is expected that complete removal of the defect would be impossible without additional feedstock, however, as this wold be a difficult extra step, the aim of this work is to reduce defect size to within tolerance rather than to completely eliminate.

Examples of defects before rework are shown in 3(a) – (d). These are all non-uniform acicular pores, as defined by shape morphology. The resulting surfaces after applying the rework strategies are shown in 3(e) – (h). A hatch pattern was applied to 3(e) and 3(f) for defects of ~350 µm and ~120 µm in diameter, respectively. The hatch rework areas show good coverage, completely encompassing the underlying defect. The individual melt tracks are visible, akin to a conventional hatch pattern in bulk

material addition. The result of a spiral rework is shown in 3(g) on a defect ~150 µm in size. Here, the resulting surface exhibits a smooth appearance with no individual melt tracks visible. A single shot rework was applied to the defect (~40 µm in size) highlighted in 3(d) and the reworked region is shown in (h), alongside a larger spiral rework. The efficacy of rework of the single shots cannot be clearly identified from the micrographs alone and a quantification of rework is necessary in order to classify these.

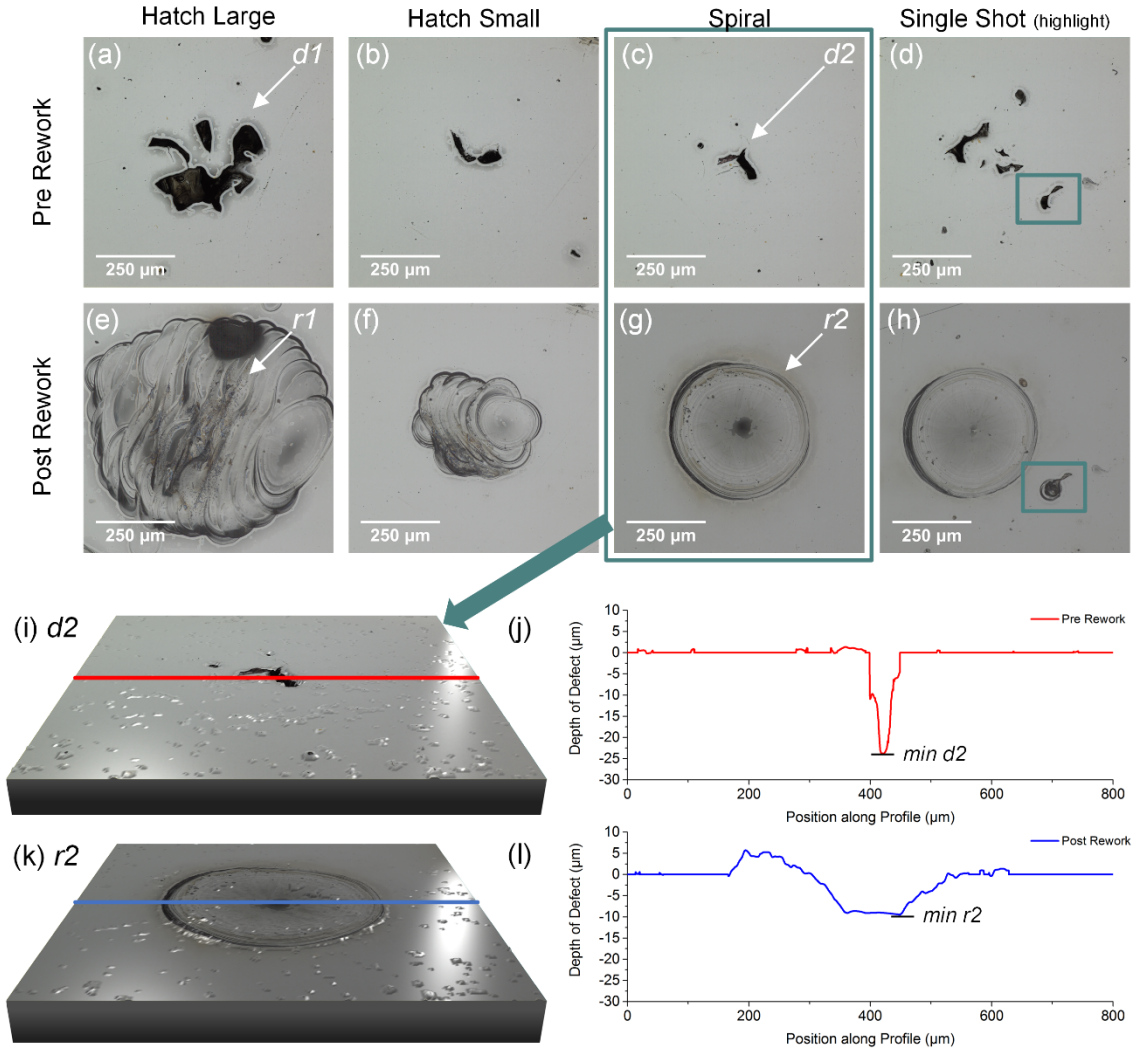

Figure 3: Optical micrographs of spherical pores of Inconel 718 samples (a) – (d) and their respective reworks (e) – (h); (e) and (f) are hatching rework strategies, (g) is a spiral rework strategy and (h) is a single shot rework. 3D views and line profiles of an exemplary pore are shown for pre rework *d2* and post rework *r2*; (i) 3D view of existing surface pore; (j) line profile through the lowest point below the surface of the pore; (k) 3D view of the reworked area; (l) line profile through the lowest point below the surface of the rework. The line profile location is marked in red and blue for the pre rework and post rework, respectively.

In order to quantitatively evaluate the effectiveness of the rework, a 3D representation of the focus variation data obtained from the defect presented in 3(c) is shown in 3(i). The corresponding 3D representation of the region after the rework is shown in 3(k). Through plotting a 2D profile through the lowest point of the dataset, a cross-sectional view of the pre-rework (3(j)) and post-rework (3(l)) can be extracted. The minimum depth of the defect pre-rework and post-rework are highlighted as *d2* and *r2*, respectively. The pre-rework profile, *d2*, exhibits a high aspect ratio similarly found in the literature [10, 32], making it difficult for subsequent powder layers to backfill this defect in the SLM manufacture. Contrary to this, it can be seen that the slopes of the reworked area, *r2*, are more normalised compared

to the initial defect. This will allow easier infill of powder particles in the next layer in the SLM manufacture. It must be noted, that through the rework operation, material has moved above the level surface to +6.3 µm. However, since the layer thickness of the SLM manufacture has been defined as 40 µm and can commonly be larger than this (> 50 µm), the material above the level surface should not impact production quality. Furthermore, a surface roughness, R_a, of ~ 5-10 µm is commonly observed in SLM [22], which is comparable with the height variation observed for the rework areas, hence the build quality for subsequent layers will remain unaffected.

Comparing *d2* and *r2*, it is seen that the rework process has also reduced the depth of the defect relative to the nominal surface. This data is presented again in 4, showing a comparison of the defect depths before rework and post rework for all three rework methodologies as extracted from line profiles through the lowest available points on all targeted rework areas. The minimum points from the profiles in 3 (j) and (l) labelled *d2* and *r2* have been transposed onto the data presented in 4 to highlight the effectiveness of reworking the targeted areas.

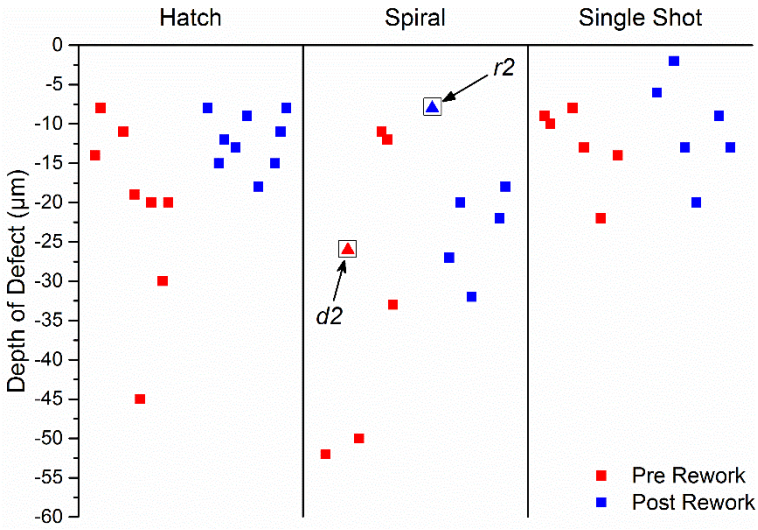

Figure 4: Plot of defect depths for all three rework methodologies; hatch, spiral and single shot (for defects smaller than 40 µm) with data shown for pre rework (red) and post rework (blue) for each. A reduction in variance can be observed for hatch and spiral rework patterns. The single shot rework patterns show no statistically relevant improvement. The minima of *r2* and *d2* are highlighted.

4, outlining the clustering of the data points, clearly demonstrates the ability of targeted re-melting to reduce the local variations in surface height caused by pores. A reduction in the depth of the defect along with a profile more favourable for infill with powder in the next build layer means that if such reworks are performed in-situ as defects develop, conditions are favourable for powder filling the defect in the next layer and the avoidance of the defect propagating through multiple layers.

Statistics of the data presented in 4 are shown in Table 1. The hatch rework methodology is shown to be more successful than the spiral method in terms of height reduction, with a higher reduction average of Δ12.1 µm (50.0%), compared to Δ9.5 µm (31.0%). The standard deviation of the data sets improved by 76.7% and 54.0% for the hatch and spiral strategies, respectively. Since Inconel 718 exhibits a relatively low thermal conductivity, the hatch pattern allows for heat dissipation outwards of the rework area, whereas the spiral rework traps the heat, which can result in over-melting at the centre, similarly reported by Jhabvala et al. [31]. A reversing of the spiral scan direction is possible and may negate the over-melting problem. However, this may result in insufficient material being moved into the defect.

The single-shot method appears to have a minimal effect on the defect depth, with an average reduction of 17.1% and an increase in the standard deviation of 22.4%. A Z-test (inverse null hypothesis) was conducted on the data sets [33], investigating the probability of rework success. This yielded a

probability of successful rework of 0.999 and 0.919 for the hatch and spiral strategies, respectively. However, the single shot repair probability of success was calculated to be 0.627 which is outside a 10% acceptable probability range (α). The low probability of success of the single shot strategy can firstly be explained by the smaller initial pore depth leaving less room for improvement and secondly by the difficulty in realignment of the specimen for the rework. The small size of the single shot reworks resulted in many of the single shots being only partially reworked, thus limiting the effectiveness of the technique, as can be seen in 3(h). The latter point can be attributed to the angular relocation accuracy of ± 0.13° in the build chamber since the measurements were conducted ex-situ and the samples needed to be relocated. This problem will be eliminated when the method is applied in-situ.

Table 1: Mean and standard deviation of defect depths as presented in 4 for both pre rework and post rework.

Repair Strategy	*Pre Depth Mean (µm)*	*Pre Depth σ (µm)*	*Post Depth Mean (µm)*	*Post Depth σ (µm)*	*Δ Mean (%)*	*Δσ (%)*	*Probability of Rework Success (P)*
Hatch	24.2	14.1	12.1	3.3	50.0	76.7	$0.9\overline{99}$
Spiral	30.7	16.3	21.2	7.5	31.0	54.0	0.919
Single Shot	12.7	4.7	10.5	5.7	17.1	-22.4	0.627

One key argument, along with the increase in processing time, for the proposed selective rework strategy as opposed to full layer re-melting, is that the latter will significantly alter the microstructure of the near surface area, a microstructure that may have been tailored for high performance functions. In order to investigate this advantage further, the effect of rework on the material surrounding a defect after rework was assessed using the SRAS instrumentation. 5 compares the SAW velocity in the bulk of the sample around the defects shown in 3, both pre and post rework. It can be seen there is a high degree of correlation between the pre and post rework results around the reworked areas with no resolvable change in microstructural texture visible. For example, the area marked *X*, shows an area of consistent velocity clusters pre and post-rework. This indicates that changes in microstructural texture are minimised by targeted re-melting. By comparison, significant microstructural changes are shown in the work by Yasa et al. after a full layer re-melt [22]. Close control of the microstructure is essential in a future, where performance metal additive manufacturing produces tailored components. A full layer re-melt could disrupt a designed microstructure whilst the targeted rework aims to reduce the impact.

Post-rework, there is an increase in unmeasurable scan points in the SRAS velocity dataset, due to the rough surface of the re-melted zones (compared with the prepared surface). With the current SRAS setup, a split photo diode is employed to obtain measurement data, which relies on a non-speckled return beam, hence rough surface detection (S_a > 500 nm) is not possible. Integration of the speckle knife edge detector will allow for rough surface detection (500 nm < S_a < 5 µm). The rough surfaces of the rework areas results from the present melt tracks. Both scans are taken at a single orientation from reference, in order to allow direct comparison of results, however this alignment was conducted manually and as SAW velocity in nickel is highly orientation dependant [29], error in alignment is likely to be the cause of the velocity variations between the two scans.

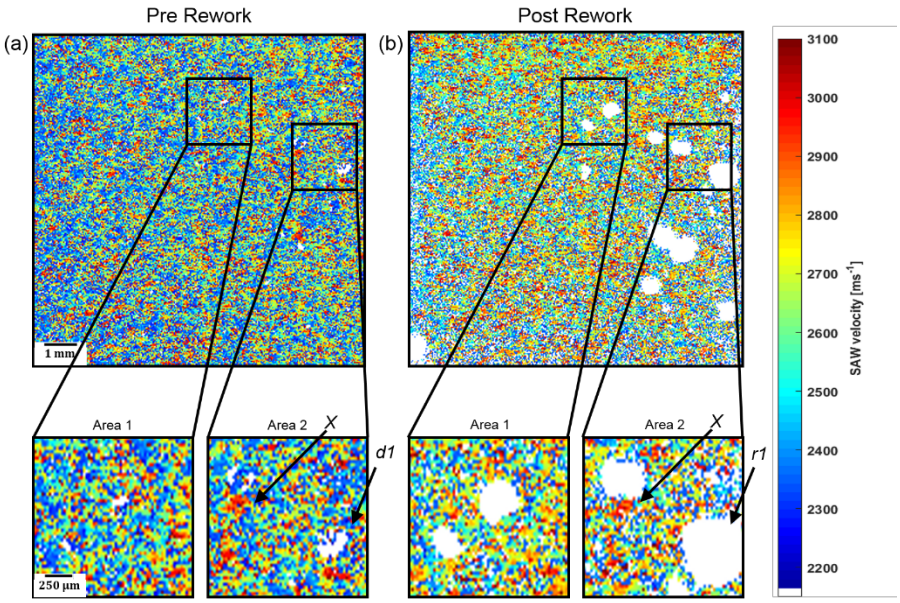

Figure 5: Comparison of SAW velocity measured by SRAS indicative of microstructural texture in the Inconel 718 sample pre rework (a) and post rework (b). Two areas are highlighted in detail for each, showing a lack of data in locations where surface defects have been observed or a rework operation has been applied. There is an increase in missing data at the reworked area, due to the rough surface arising from the re-melting of the surface. *d1* and *r1* are highlighted in Area 2. Exemplary clustering of consistent velocity between pre- and post-rework are indicated by *X* to aid interpretation. The scale bars for a) and b) are 1 mm and 250 µm for the zoomed sections.

The workflow developed in this study has been tested on Inconel 718 manufactured by SLM but can be generalised such that this technique can easily be applied to other AM/3D printing processes; this is shown in 6. This build-characterise-rework strategy allows for integration of a measurement technique and repair strategies within an AM build environment to allow targeted reworked on a layer by layer basis. A layer of the additive manufacture is illustrated in 6(a), followed by component measurement 6(b), decision on cancelling the build in 6(c), rework path definition in 6(d), applying the rework and verify in 6(e), with the final part completed at the end in 6(f). Application of this technique in-situ necessitates a deviation from current practice, where scan paths are fixed pre-build. Instead integration of the path generation algorithm described in this work into the build controller shall allow for dynamic generation of scan paths, based on inspection, as necessary for rework.

An example application of this methodology, aside from SLM, is in-situ cell repair in tissue printing systems [34], where Brillouin oscillation imaging [35] could be employed to verify the quality of printed tissue. Another example of this workflow being employed is in the automotive industry where polymer based AM processes are used for interior trim applications [36]. A suitable in-situ measurement process, such as optical coherence tomography for selective laser sintering [37], could be used to inform on rework strategies in production for part quality optimisation in this highly aesthetic application. The long term aim of this work is to develop an automated system that is capable of the in-process identification, characterisation and rework of defects occurring in an SLM build. The benefits of this approach include reducing cost of production, reduction in waste of failed parts and optimisation of the production chain by reducing the need for additional post process part evaluation.

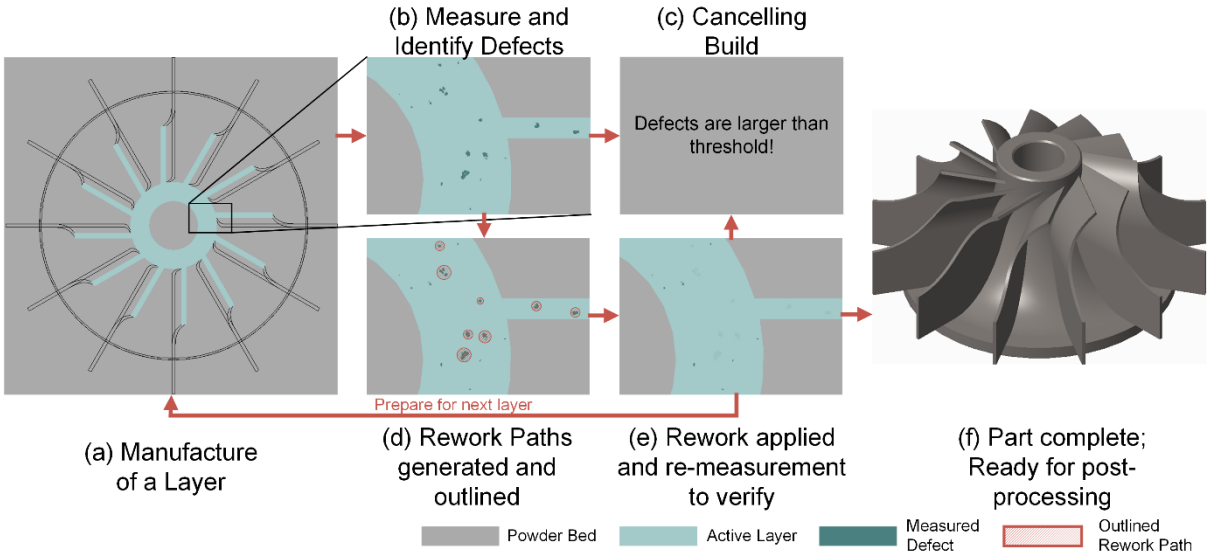

Figure 6: Flowchart of proposed targeted rework approach simulated in this work. (a) outlines the completed processing of an SLM layer; (b) shows a measurement step, where defects are identified and it is determined to either cancel the build or to rework the defects; (c) if the defects are above a predefined threshold, the build may be cancelled; (d) if below threshold, through data processing, rework paths can be defined for (e) targeted re-melting with the option of re-measurement to, again, cancel, or continue manufacture; This process may repeat on a layer per layer basis with the finished part shown in (f).

4. Conclusions

The work presented in this paper has shown that targeted rework of a nickel superalloy SLM component surface is a feasible approach to reducing porosity defects. Three laser scan strategies were trialled in order to rework non-artificial defects: hatch, spiral and one-shot (for defects below 40 µm). Some rework techniques were shown to successfully rework the pores and reduce the variation in depths across the defect, with the hatch technique proving to be the most effective, a defect depth improvement of 50.00% was achieved on average. The treated areas also undergo a change in morphology that increases the defect slope angle; this would give a better opportunity for backfill with powder when subsequent layers are manufactured.

The methodology of rework demonstrated in this paper is highly suitable for integration into an entirely in-situ system, as measurements can be made within a modified SLM laser/optics system, rework scan paths can be computed on-the-fly, and the rework paths can be applied within the same manufacturing process with little increase in build time. Whilst this study has focussed on targeted surface rework, the advent of in-situ inspection would allow for re-melting to occur throughout the build-process in order to rework defects within the build volume of the component.

Acknowledgements

This work was supported by the Engineering and Physical Sciences Research Council [grant number EP/L022125/1] through the ‘UK Research Centre in Nondestructive Evaluation’. The authors acknowledge Alexander Gasper (Advanced Component Engineering Laboratory, University of Nottingham) for assistance in Inconel 718 sample manufacture and preparation. We would like to thank the Centre for Additive Manufacture (University of Nottingham) for enabling us to additively manufacture the specimen.

References

[1] B.P. Conner, G.P. Manogharan, A.N. Martof, L.M. Rodomsky, C.M. Rodomsky, D.C. Jordan, J.W. Limperos, Making sense of 3-D printing: Creating a map of additive manufacturing products and services, Additive Manufacturing 1–4 (2014) 64-76.
[2] F. Abe, K. Osakada, M. Shiomi, K. Uematsu, M. Matsumuto, The manufacturing of hard tools from metallic powders by selective laser melting, Journal of Materials Processing Technology 111(1-3) (2001) 210-213.
[3] A. Voet, J. Mingneau, J. Dehaes, J.-P. Kruth, v.J. Vaerenbergh, Study of the wear behaviour of conventional and rapid tooling mould materials, International Conference Polymers & Moulds Innovations PMI, Gent, Belgium, 2005.
[4] F.P.W. Melchels, M.A.N. Domingos, T.J. Klein, J. Malda, P.J. Bartolo, D.W. Hutmacher, Additive manufacturing of tissues and organs, Progress in Polymer Science 37(8) (2012) 1079-1104.
[5] T. Caffrey, I. Campbell, T. Wohlers, Wohlers Report 2016: Additive Manufacturing and 3D Printing State of the Industry, Annual Worldwide Progress Report, Wohlers Associates, Inc, Fort Collins, 2016.
[6] P. Edwards, A. O'Conner, M. Ramulu, Electron Beam Additive Manufacturing of Titanium Components: Properties and Performance, Journal of Manufacturing Science and Engineering 135(6) (2013) 061016.
[7] M. Fousová, D. Vojtěch, J. Kubásek, E. Jablonská, J. Fojt, Promising characteristics of gradient porosity Ti-6Al-4V alloy prepared by SLM process, Journal of the Mechanical Behavior of Biomedical Materials 69(Supplement C) (2017) 368-376.
[8] S. Leuders, M. Thöne, A. Riemer, T. Niendorf, T. Tröster, H.A. Richard, H.J. Maier, On the mechanical behaviour of titanium alloy TiAl6V4 manufactured by selective laser melting: Fatigue resistance and crack growth performance, International Journal of Fatigue 48 (2013) 300-307.
[9] S.K. Everton, M. Hirsch, P. Stravroulakis, R.K. Leach, A.T. Clare, Review of in-situ process monitoring and in-situ metrology for metal additive manufacturing, Materials & Design (2016).
[10] S. Tammas-Williams, H. Zhao, F. Léonard, F. Derguti, I. Todd, P.B. Prangnell, XCT analysis of the influence of melt strategies on defect population in Ti–6Al–4V components manufactured by Selective Electron Beam Melting, Materials Characterization 102 (2015) 47-61.
[11] K. Darvish, Z.W. Chen, T. Pasang, Reducing lack of fusion during selective laser melting of CoCrMo alloy: Effect of laser power on geometrical features of tracks, Materials & Design 112 (2016) 357-366.
[12] C.L. Qiu, N.J.E. Adkins, M.M. Attallah, Microstructure and tensile properties of selectively laser-melted and of HIPed laser-melted Ti-6Al-4V, Mat Sci Eng a-Struct 578 (2013) 230-239.
[13] K. Murali, A.N. Chatterjee, P. Saha, R. Palai, S. Kumar, S.K. Roy, P.K. Mishra, A.R. Choudhury, Direct selective laser sintering of iron-graphite powder mixture, Journal of Materials Processing Technology 136(1-3) (2003) 179-185.
[14] M.J. Matthews, G. Guss, S.A. Khairallah, A.M. Rubenchik, P.J. Depond, W.E. King, Denudation of metal powder layers in laser powder bed fusion processes, Acta Materialia 114(Supplement C) (2016) 33-42.
[15] M. Hirsch, R. Patel, W. Li, G. Guan, R.K. Leach, S.D. Sharples, A.T. Clare, Assessing the capability of in-situ nondestructive analysis during layer based additive manufacture, Additive Manufacturing 13 (2017) 135-142.
[16] M. Van Elsen, Complexity of Selective Laser Melting: A New Optimisation Approach 'Katholieke Universiteit Leuven, Belgium, 2007.
[17] S.A. Khairallah, A.T. Anderson, A. Rubenchik, W.E. King, Laser powder-bed fusion additive manufacturing: Physics of complex melt flow and formation mechanisms of pores, spatter, and denudation zones, Acta Materialia 108 (2016) 36-45.
[18] S. Tammas-Williams, P.J. Withers, I. Todd, P.B. Prangnell, The Effectiveness of Hot Isostatic Pressing for Closing Porosity in Titanium Parts Manufactured by Selective Electron Beam Melting, Metallurgical and Materials Transactions A 47(5) (2016) 1939-1946.
[19] L.E. Murr, E. Martinez, S.M. Gaytan, D.A. Ramirez, B.I. Machado, P.W. Shindo, J.L. Martinez, F. Medina, J. Wooten, D. Ciscel, U. Ackelid, R.B. Wicker, Microstructural Architecture, Microstructures, and Mechanical Properties for a Nickel-Base Superalloy Fabricated by Electron Beam Melting, Metallurgical and Materials Transactions A 42(11) (2011) 3491-3508.
[20] J. Grum, J.M. Slabe, Possibility of introducing laser surfacing into maintenance service of die-casting dies, Surface and Coatings Technology 180-181 (2004) 596-602.

[21] P. Mercelis, J.P. Kruth, Residual stresses in selective laser sintering and selective laser melting, Rapid Prototyping Journal 12(5) (2006) 254-265.
[22] E. Yasa, J. Deckers, J.P. Kruth, The investigation of the influence of laser re‐melting on density, surface quality and microstructure of selective laser melting parts, Rapid Prototyping Journal 17(5) (2011) 312-327.
[23] T.R. Newton, S.N. Melkote, T.R. Watkins, R.M. Trejo, L. Reister, Investigation of the effect of process parameters on the formation and characteristics of recast layer in wire-EDM of Inconel 718, Mat Sci Eng a-Struct 513-14 (2009) 208-215.
[24] J. Mireles, S. Ridwan, P.A. Morton, A. Hinojos, R.B. Wicker, Analysis and correction of defects within parts fabricated using powder bed fusion technology, Surface Topography: Metrology and Properties 3(3) (2015) 034002.
[25] M. Hirsch, S. Catchpole-Smith, R. Patel, P. Marrow, W. Li, C. Tuck, S.D. Sharples, A.T. Clare, Meso-scale defect evaluation of selective laser melting using spatially resolved acoustic spectroscopy, Proc. R. Soc. A, The Royal Society, 2017, p. 20170194.
[26] R.J. Smith, M. Hirsch, R. Patel, W. Li, A.T. Clare, S.D. Sharples, Spatially Resolved Acoustic Spectroscopy for Selective Laser Melting, Journal of Materials Processing Technology (2016).
[27] S.D. Sharples, R.A. Light, S.O. Achamfuo-Yeboah, M. Clark, M.G. Somekh, The SKED: speckle knife edge detector, Journal of Physics: Conference Series 520 (2014) 012004.
[28] R.J. Smith, W. Li, J. Coulson, M. Clark, M.G. Somekh, S.D. Sharples, Spatially resolved acoustic spectroscopy for rapid imaging of material microstructure and grain orientation, Measurement Science and Technology 25(5) (2014) 055902.
[29] W. Li, J. Coulson, J.W. Aveson, R.J. Smith, M. Clark, M.G. Somekh, S.D. Sharples, Orientation Characterisation of Aerospace Materials by Spatially Resolved Acoustic Spectroscopy, Journal of Physics: Conference Series 520 (2014) 012017.
[30] M. Rahman, W.K.H. Seah, T.T. Teo, The machinability of Inconel 718, Journal of Materials Processing Technology 63(1-3) (1997) 199-204.
[31] J. Jhabvala, E. Boillat, T. Antignac, R. Glardon, On the effect of scanning strategies in the selective laser melting process, Virtual and Physical Prototyping 5(2) (2010) 99-109.
[32] C. Panwisawas, C.L. Qiu, Y. Sovani, J.W. Brooks, M.M. Attallah, H.C. Basoalto, On the role of thermal fluid dynamics into the evolution of porosity during selective laser melting, Scripta Materialia 105(Supplement C) (2015) 14-17.
[33] D.C. Montgomery, G.C. Runger, N.F. Hubele, Engineering statistics, John Wiley & Sons2009.
[34] V. Mironov, T. Boland, T. Trusk, G. Forgacs, R.R. Markwald, Organ printing: computer-aided jet-based 3D tissue engineering, Trends Biotechnol 21(4) (2003) 157-161.
[35] F. Perez-Cota, R.J. Smith, E. Moradi, L. Marques, K.F. Webb, M. Clark, Thin-film optoacoustic transducers for subcellular Brillouin oscillation imaging of individual biological cells, Appl Optics 54(28) (2015) 8388-8398.
[36] C.A. Giffi, B. Gangula, P. Illinda, 3D opportunity in the automotive industry: Additive manufacturing hits the road (White Paper), Deloitte Development LLC, 2014, pp. 1-28.
[37] G. Guan, M. Hirsch, Z.H. Lu, D.T.D. Childs, S.J. Matcher, R. Goodridge, K.M. Groom, A.T. Clare, Evaluation of selective laser sintering processes by optical coherence tomography, Materials & Design 88 (2015) 837-846.